PHILOSOPHICAL TRANSACTIONS B

royalsocietypublishing.org/journal/rstb

Research

Cite this article: Childs ML, Nova N, Colvin J, Mordecai EA. 2019 Mosquito and primate ecology predict human risk of yellow fever virus spillover in Brazil. *Phil. Trans. R. Soc. B* **374**: 20180335.
http://dx.doi.org/10.1098/rstb.2018.0335

Accepted: 29 April 2019

One contribution of 20 to a theme issue 'Dynamic and integrative approaches to understanding pathogen spillover'.

Subject Areas:
ecology, health and disease and epidemiology, computational biology

Keywords:
Brazil, disease ecology, mosquito, pathogen spillover, vector-borne disease, yellow fever

Author for correspondence:
Marissa L. Childs
e-mail: marissac@stanford.edu

Electronic supplementary material is available online at https://dx.doi.org/10.6084/m9.figshare.c.4555469.

THE ROYAL SOCIETY PUBLISHING

Mosquito and primate ecology predict human risk of yellow fever virus spillover in Brazil

Marissa L. Childs[1], Nicole Nova[2], Justine Colvin[2] and Erin A. Mordecai[2]

[1]Emmett Interdisciplinary Program in Environment and Resources, and [2]Department of Biology, Stanford University, Stanford, CA 94305, USA

MLC, 0000-0002-8597-2161; NN, 0000-0001-8585-1215; EAM, 0000-0002-4402-5547

Many (re)emerging infectious diseases in humans arise from pathogen spillover from wildlife or livestock, and accurately predicting pathogen spillover is an important public health goal. In the Americas, yellow fever in humans primarily occurs following spillover from non-human primates via mosquitoes. Predicting yellow fever spillover can improve public health responses through vector control and mass vaccination. Here, we develop and test a mechanistic model of pathogen spillover to predict human risk for yellow fever in Brazil. This environmental risk model, based on the ecology of mosquito vectors and non-human primate hosts, distinguished municipality-months with yellow fever spillover from 2001 to 2016 with high accuracy (AUC = 0.72). Incorporating hypothesized cyclical dynamics of infected primates improved accuracy (AUC = 0.79). Using boosted regression trees to identify gaps in the mechanistic model, we found that important predictors include current and one-month lagged environmental risk, vaccine coverage, population density, temperature and precipitation. More broadly, we show that for a widespread human viral pathogen, the ecological interactions between environment, vectors, reservoir hosts and humans can predict spillover with surprising accuracy, suggesting the potential to improve preventive action to reduce yellow fever spillover and avert onward epidemics in humans.

This article is part of the theme issue 'Dynamic and integrative approaches to understanding pathogen spillover'.

1. Introduction

Many important (re)emerging infectious diseases in humans—including Ebola, sudden acute respiratory syndrome (SARS), influenza, *Plasmodium knowlesi* and other primate malarias, yellow fever and leptospirosis—arise from spillover of pathogens from wildlife or livestock into human populations [1,2]. While spillover is an important mechanism of human disease emergence, the drivers and dynamics of spillover are poorly understood and difficult to predict [3]. Pathogen spillover requires favourable conditions to align in the reservoir (non-human animal), human and pathogen populations and in the environment [3–5]. Because these conditions interact, nonlinear relationships among the environment, host populations and spillover probability are likely to emerge. Moreover, spillover is a probabilistic process that does not always occur, even when suitable conditions align. Despite these challenges, it is critical to predict pathogen spillover to enhance public health preparedness. Predicting spillover also provides an opportunity to test ecological approaches to solving globally important human health problems.

Most previous attempts to predict pathogen spillover have used statistical models [6–8]. These models may be locally accurate for within-sample prediction, but may struggle to detect multidimensional, nonlinear and stochastic relationships among host populations, pathogens, the environment and spillover.

By contrast, mechanistic models can test our understanding of transmission ecology, reproduce the complex, nonlinear interactions emerging in disease systems and potentially improve our ability to predict spillover. In particular, Plowright *et al.* [3] recently proposed a mechanistic model, which remains untested, that integrates multiple ecological requirements to identify when conditions will align for pathogen spillover. Yellow fever in Brazil presents an ideal opportunity to test this model because the ecology of the pathogen has been studied for nearly 120 years [9], providing a wealth of mechanistic information and data, and because almost all recent cases in South America have occurred via spillover from the sylvatic cycle [10,11].

Yellow fever virus is a mosquito-borne *Flavivirus* that mainly persists in a sylvatic transmission cycle between forest mosquitoes (primarily *Haemagogus janthinomys*, *Hg. leucocelaenus* and *Sabethes chloropterus* in South America) and non-human primates, and occasionally spills over into human populations [12]. In some settings, these spillover events lead to onward human epidemics in an urban transmission cycle between humans and *Aedes aegypti* mosquitoes [9]. Spillover of yellow fever requires the virus to be transmitted locally, mosquito vectors to acquire the virus from infected non-human vertebrate hosts, survive the extrinsic incubation period, and feed on human hosts, and human hosts to be susceptible to infection following exposure. These events require distributions of reservoirs, vectors and humans, their interactions, and immune dynamics to align in space and time. In humans, yellow fever is the most severe vector-borne virus circulating in the Americas [10], with an estimated fatality rate for severe cases of 47% [13]. While no urban transmission of yellow fever has occurred in the Americas since 1997 [14] and in Brazil since 1942 [15], a large epidemic began in December 2016 in Minas Gerais and by June 2018 had caused 2154 confirmed cases and 745 deaths [16]. Despite these large case numbers, molecular and epidemiological evidence suggests that human cases were caused by spillover from the sylvatic cycle, rather than urban transmission [11], most recently in areas previously believed to be free of yellow fever.

Prior statistical models have found climate and weather (including precipitation, temperature and normalized difference vegetation index), non-human primate richness, land use intensiveness and a latitudinal gradient to be predictive of the spatial and spatio-temporal distribution of yellow fever [6,8]. We build on previous efforts by incorporating a mechanistic understanding of how ecological and human population factors affect yellow fever transmission and spillover. A mechanistic model allows known relationships between the environment and transmission mechanisms, estimated from empirical data, to be included to test our understanding of the disease ecology. Additionally, mechanistic models allow extrapolation beyond known regions to identify other regions where conditions are also suitable for yellow fever spillover. We use a mechanistic model encapsulating sylvatic yellow fever ecology to predict the spatial and temporal distribution of yellow fever spillover in Brazil, and we test the model on human yellow fever case data using a receiver operating characteristic curve and logistic regression. Here, we use 'predict' to refer to independently estimating spillover risk mechanistically from simultaneous covariates and 'forward prediction' to refer to estimating future spillover. We contrast this mechanistic prediction with statistical models that are fitted to the spillover data, and therefore not able to make independent, out-of-sample predictions. We then incorporate the mechanistic model into further statistical analyses with boosted regression trees to understand what mechanisms our model does not capture.

Specifically, we ask: (1) Does the environmental suitability for sylvatic vectors, reservoir hosts, vector–human contact and vector transmission—together termed environmental risk—predict geographical, seasonal and interannual variation in yellow fever virus spillover into humans? (2) Are human population size and vaccine coverage, above and beyond environmental risk, critical for predicting spillover? (3) What additional environmental and population drivers might improve predictions of spillover? (4) Do the ecological processes that predict spillover in other parts of Brazil predict the recent yellow fever outbreak in the Southeast region of Brazil in 2016–2018, and if so, was risk elevated above historical baseline levels?

2. Methods

Our goals were (1) to construct mechanistic estimates of yellow fever spillover risk over space and time, (2) to test these mechanistic risk models against observed cases of yellow fever spillover to humans and (3) to statistically test for associations between observed spillover occurrence, mechanistically predicted risk and environmental covariates to identify potential gaps in the mechanistic models. We constructed mechanistic risk estimates by modelling the ecological processes expected to drive transmission within reservoir hosts—vector distribution and seasonal abundance, vector dispersal, vector infectiousness, vector survival, vector–reservoir contact and reservoir host distributions—and the risk of spillover to humans—human population density, vector–human contact rates and human susceptibility (figure 1, Mechanistic model). For each of these ecological or human population factors, we parameterized a submodel using data from the literature and remotely sensed covariates (figure 1 lists data sources and figure 2 shows the data and/or fitted submodels). We modelled several different risk metrics, as described below (see Methods: Spillover model (§2a)). We then predicted monthly risk of yellow fever spillover from the component submodels for each 1 km × 1 km pixel from December 2000 to December 2016 (figure 1; electronic supplementary material, S1.1). The risk estimates from January 2001 to December 2016 were aggregated to a municipality-level estimate to compare with available reports of human cases. Next, to test for relationships that were absent or mis-specified in our mechanistic model, we used both current and lagged aggregated municipality-wide environmental risk from December 2000 to December 2016 as covariates in a statistical model (a boosted regression tree) along with other environmental and demographic covariates to identify the traits of municipalities and months when yellow fever spillover occurred using the available human case data from 2001 to 2016 (figure 1, Statistical model). Finally, we sought to identify whether the mechanistic models predicted high suitability for spillover during the recent outbreaks (December 2016–April 2018) [16]. Given the limited time range of some covariates, we extrapolated model covariates for 2017 and 2018 by assuming that they were identical to 2016 or followed the same linear trend as was observed from 2015 to 2016. We then calculated the environmental risk metric for January 2017 to June 2018 in the region where the large outbreak occurred.

(a) Spillover model

Yellow fever spillover risk was first estimated monthly from December 2000 to December 2016 using an adapted version of

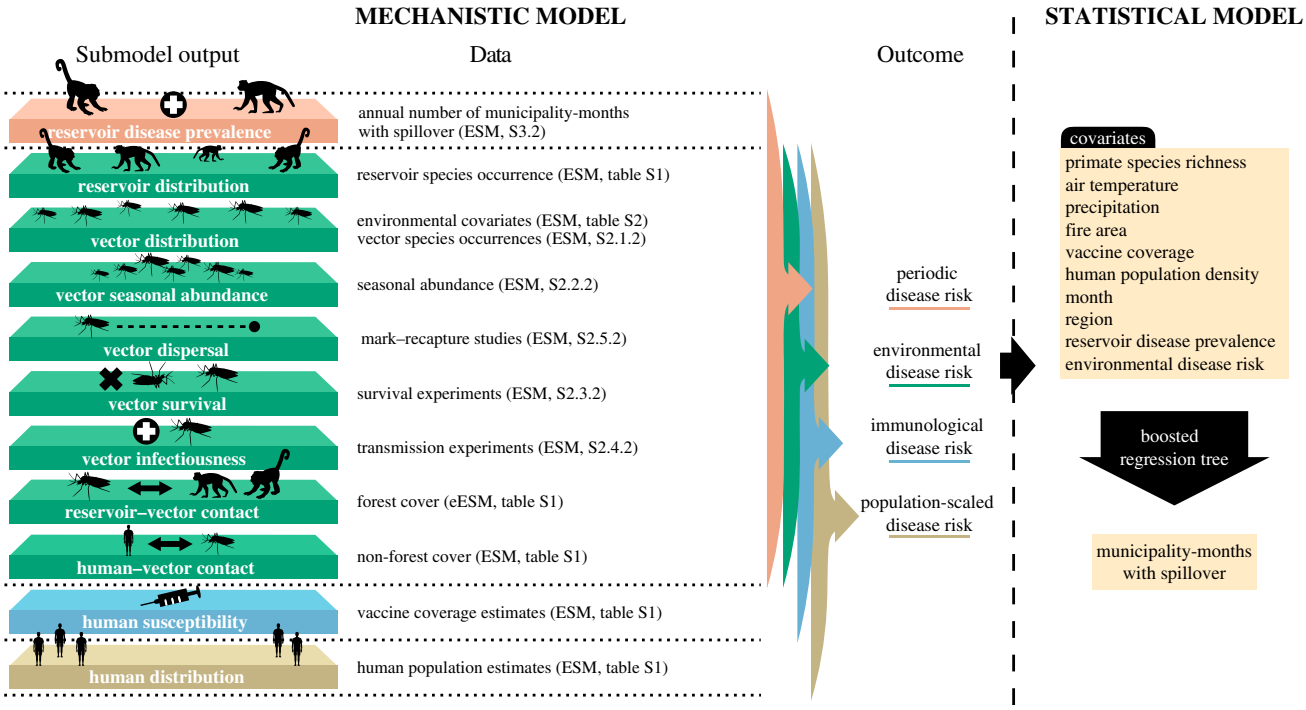

Figure 1. Mechanistic and statistical model schematic. Submodels of components in the mechanistic model are parameterized using independent data on reservoir species, vector species occurrences, seasonal abundances, vector mark–recapture studies, vector survival, transmission experiments, forest cover, estimated vaccine coverage and human population estimates. Reservoir disease prevalence is estimated from annual number of municipality-months with spillover. The output from the submodels are used in a mechanistic spillover model to predict four risk metrics of yellow fever in humans: periodic disease risk, environmental disease risk, immunological disease risk, and population-scaled disease risk. Environmental disease risk metric is then used as a covariate in a boosted regression tree to predict the municipality-months with spillover and identify covariates important for predicting spillover. Other environmental covariates are also included in the boosted regression tree. Details on data used in the mechanistic model can be found in the electronic supplementary material (ESM). Specific locations within the electronic supplementary material are noted parenthetically by either the section or table in which details can be found. Data used in the boosted regression tree are described in electronic supplementary material, table S6. Layers shown on the left correspond to mechanistic model components in figure 2*a–k*.

the model from Plowright *et al.* [3]. We then estimated monthly spillover risk using extrapolated covariates (electronic supplementary material, table S1) for the duration of the 2016–2018 outbreaks. We defined environmental risk at a location $\boldsymbol{y}$ and time t—proportional to the number of infectious mosquito bites—as:

$$b(\boldsymbol{y},t)\beta_{\mathrm{h}}(\boldsymbol{y},t)\int_{\tau=0}^{\tau=t}\int_{\vec{x}}\rho_{\mathrm{v}}(\boldsymbol{x},\tau)b(\boldsymbol{x},\tau)\beta_{\mathrm{p}}(\boldsymbol{x},\tau)\kappa(\boldsymbol{x},\tau)\mathrm{EIP}(T(\boldsymbol{x},\tau),\,t-\tau)$$
$$\times s(T(\boldsymbol{x},\tau),\,t-\tau)d(\|\boldsymbol{y}-\boldsymbol{x}\|)\mathrm{d}x\mathrm{d}\tau, \qquad (2.1)$$

as a function of sylvatic vector density ($\rho_{\mathrm{v}}(\boldsymbol{x},t)$, figure 2*b*,*e*), probability of biting non-human primates ($\beta_{\mathrm{p}}(\boldsymbol{x},t)$, figure 2*c*) contingent on primate presence (figure 2*a*), probability of biting humans ($\beta_{\mathrm{h}}(\boldsymbol{y},t)$, figure 2*d*) which depends on human presence (figure 2*j*), non-human primate infection prevalence ($\kappa(\boldsymbol{x},\tau)$, figure 2*k*), vector biting rate ($b(\boldsymbol{y},t)$), vector probability of becoming infectious ($\mathrm{EIP}(T(\boldsymbol{x},t),\,t-\tau)$, figure 2*h*), vector survival ($s(T(\boldsymbol{x},\tau),\,t-\tau)$, figure 2*g*) and vector dispersal ($d(\|\boldsymbol{y}-\boldsymbol{x}\|)$, figure 2*f*), as described in table 1. This model is a case study of a more general family of percolation models of pathogen spillover with alternative pathogen sources in space and time [17].

We hypothesized that yellow fever spillover could be limited by environmental conditions, human susceptibility, human population distribution and primate infection dynamics. To compare their relative importance, we defined four metrics of model-predicted yellow fever spillover risk. First, we approximated *environmental risk* (equation (2.1), figure 2*l*), assuming that biting rate ($b(\boldsymbol{y},t)$ in equation (2.1)) and reservoir infection prevalence ($\kappa(\boldsymbol{x},\tau)$ in equation (2.1)) are constant over space and time in the absence of empirical data on these parameters, as described in table 1. Since this metric ignores variation in human susceptibility, we then calculated *immunological risk* (figure 2*m*) as environmental risk multiplied by the estimated proportion of the human population that is susceptible to yellow fever (figure 2*i*), using previously estimated vaccine coverage rates [18]. We then considered the influence of human population size on spillover risk by calculating *population-scaled risk* (figure 2*n*) as the immunological risk scaled by the number of people in a given location (figure 2*j*). Finally, we incorporated the effects of cycles of reservoir susceptibility and infection dynamics, for which data were not available, by calculating *periodic risk* (figure 2*o*), which uses a phenomenological periodic curve (figure 2*k*) for primate infection prevalence ($\kappa(\boldsymbol{x},\tau)$ in equation (2.1)). This periodic curve was designed to represent cycles of reservoir infection prevalence, driven by the demography of primate populations as naive individuals are born, susceptible individuals accumulate, and epizootics become more likely [19]. The full spillover model was run in Google Earth Engine [20]. We estimated risk metrics monthly for 1 × 1 km pixels using built-in functionality of Google Earth Engine that allows calculations across differing scales by performing calculations for a specified output pixel scale.

(b) Mechanistic submodels

We fitted mechanistic submodels from data for all key components of spillover (figure 1). For primate distribution (figure 2*a*), human susceptibility (figure 2*i*) and human population distribution (figure 2*j*), we used previously published estimates [18,21,22]. All other mechanistic models (terms in equation (2.1)) were fitted with the R programming language, v.3.5.1 [23], with additional packages used for data processing, manipulation and visualization [24–32].

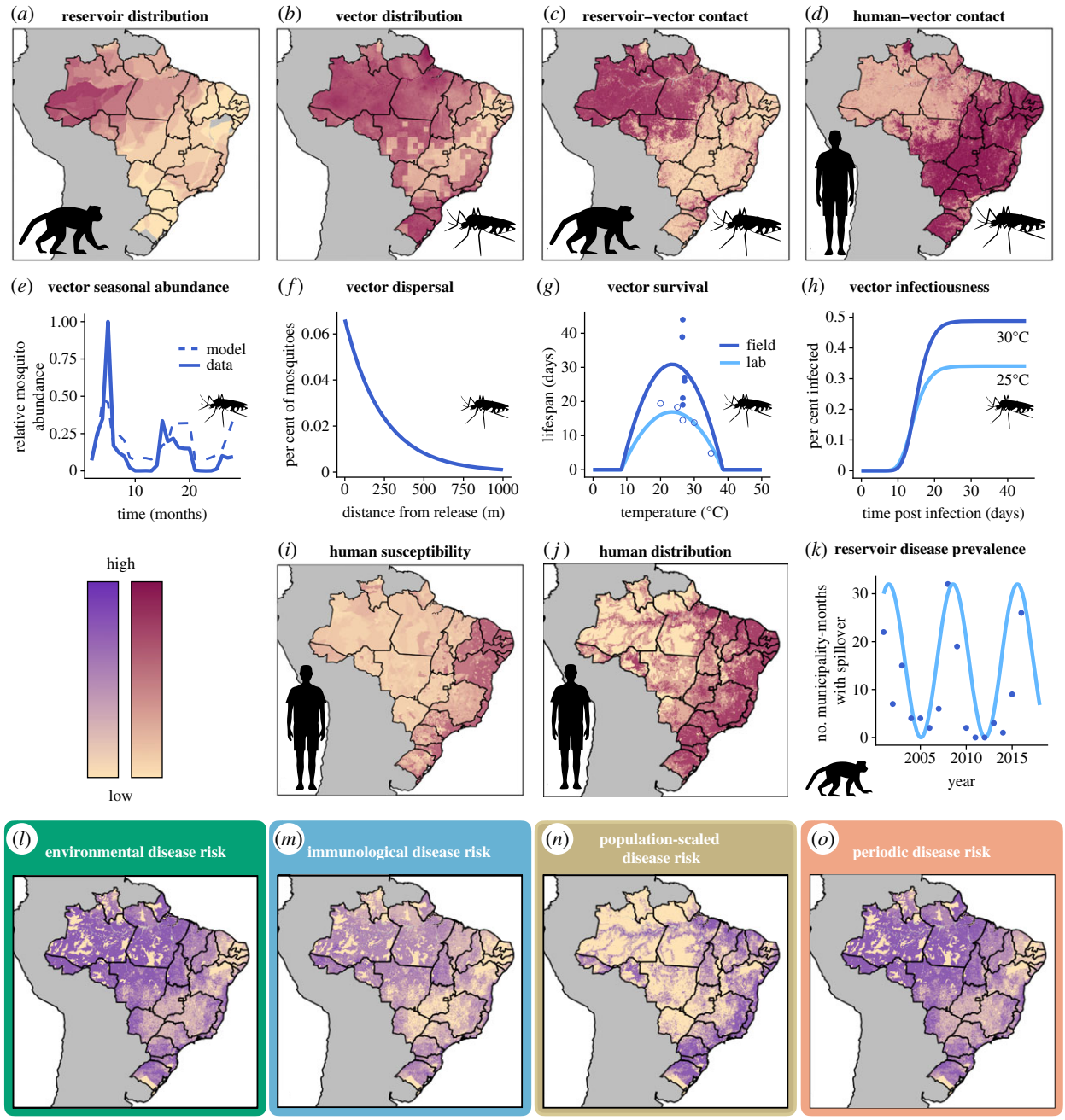

Figure 2. Data used to estimate ecological and human population components of spillover (*a*–*k*) and estimates of overall spillover risk (*l*–*o*). Number of primate reservoir species (*a*), vector species probability of occurrence (*b*), reservoir–vector contact probability (*c*), human–vector contact probability (*d*), human susceptibility approximated by 1 minus estimated vaccine coverage (*i*), and human distribution (*j*) vary spatially. Vector seasonal abundance is modelled as a function of rainfall using mosquito capture data (*e*). Vector dispersal depends on distance and is estimated from mark–recapture studies (*f*). Vector survival has been measured at different temperatures in laboratory (open circles) and field (closed circles) settings and was used to estimate temperature-dependent vector lifespan (*g*). Transmission studies at different temperatures inform modelled probability of vector infectiousness as a function of days since infecting bite and temperature (*h*). Phenomenologically modelled reservoir disease prevalence (light blue line, *k*) is approximated from human case data (blue dots, *k*). All mechanistic model components (*a*–*k*) are derived from empirical data in previously published studies. Components *a*–*h* are used to predict environmental risk of disease spillover (*l*), components *a*–*i* are used for immunological risk (*m*), components *a*–*j* are used for population-scaled risk (*n*) and components *a*–*h* and *k* are used for periodic risk (*o*). The four disease risk metrics presented here for illustrative purposes were estimated for January 2001 (*l*–*o*). (Online version in colour.)

Given limited information on the vector species, we used data for *Hg. janthinomys*, *Hg. leucocelaenus* and *Sa. chloropterus* to fit models for the sylvatic vectors collectively for all mechanistic vector trait models. All data used were publicly available or results from previously published papers, as described in electronic supplementary material, S2 and table S1. Additional details on mechanistic model methods and data are available in the electronic supplementary material.

(i) Vector distribution and seasonal density

To estimate the geographical distribution of sylvatic vector species (figure 2*b*), we fitted a species distribution model [33,34] to *Hg. janthinomys*, *Hg. leucocelaenus* and *Sa. chloropterus* occurrence data identified from the Global Biodiversity Information Facility (GBIF) [35–37] and a review of the literature [38–92], using the maxnet package in R [93]. We included maximum, median and minimum annual land surface temperature,

Table 1. Spillover model variables and definitions.

variable	definition	model
$\beta_h(\boldsymbol{x},t)$	proportion of mosquito bites from sylvatic vectors on humans at location $\boldsymbol{x}$ at time t	approximated as $1 - f(\boldsymbol{x},t)$ in locations with non-zero human population density, where $f(\boldsymbol{x},t)$ is the per cent forest cover at location $\boldsymbol{x}$ at time t
$\beta_p(\boldsymbol{x},t)$	proportion of mosquito bites from sylvatic vectors on non-human primates at location $\boldsymbol{x}$ at time t	approximated as $f(\boldsymbol{x},t)$ in locations within at least one non-human primate range, where $f(\boldsymbol{x},t)$ is the per cent forest cover at location $\boldsymbol{x}$ at time t
$\rho_v(\boldsymbol{x},t)$	sylvatic vector density at location $\boldsymbol{x}$ at time t	approximated as maximum mosquito density in a location multiplied by relative seasonal abundance, where maximum mosquito density is determined by a species distribution model and seasonal abundance is modelled from field capture data (see Methods: Mechanistic models—Vector distribution and seasonal density (§2b(i)))
$\mathrm{EIP}(T(\boldsymbol{x},t),\Delta t)$	probability a mosquito that took an infectious blood meal becomes infectious with yellow fever virus given a temperature $T(\boldsymbol{x},t)$ and Δt days elapsing	see Methods: Mechanistic submodels—Vector infectiousness (§2b(iii))
$s(T(\boldsymbol{x},t),\Delta t)$	probability that a mosquito survives Δt days given a temperature $T(\boldsymbol{x},t)$	see Methods: Mechanistic submodels—Vector survival (§2b(ii))
$d(\lVert\boldsymbol{x} - \boldsymbol{y}\rVert)$	probability that a mosquito disperses from $\boldsymbol{x}$ to $\boldsymbol{y}$	see Methods: Mechanistic submodels—Vector dispersal (§2b(iv))
$b(\boldsymbol{x},t)$	biting rate of sylvatic vectors at location $\boldsymbol{x}$ at time t	assumed constant given limited information on determinants of vector biting rates
$\kappa(\boldsymbol{x},t)$	infection prevalence in non-human primate reservoir at location $\boldsymbol{x}$ at time t	for environmental risk metric, assumed constant given limited information of non-human primate infection prevalence. For periodic risk metric, used periodic curve fitted to yearly case data (see Methods: Phenomenological primate dynamics (§2c)).

total annual precipitation, precipitation in the driest month, precipitation in the wettest month, elevation, forest cover (%), land cover category, median annual enhanced vegetation index and absolute latitude as predictors in the model (electronic supplementary material, table S2). To account for uneven sampling effort across the geographical range, we corrected the background (pseudo-absence) points by subsampling from occurrence data of other mosquito species from GBIF [94]. We calculated vector density as $\log(1/(1-p))$, where p is the probability of occurrence estimated from the species distribution model [95]. To estimate seasonal variation in vector abundance (figure 2*e*) due to rainfall seasonality [96], we fitted a logistic regression of relative monthly vector abundance on current and one-month lagged relative monthly rainfall using field data [60,82,97–100] with glm in R.

(ii) Vector survival

To capture effects of temperature on vector survival (figure 2*f*), we used empirical data [101–103] and Bayesian inference to fit a quadratic function to the relationship between lifespan and temperature using RStan in R [104]. Assuming constant vector mortality at a given temperature, we calculated daily survival probability as $p = \mathrm{e}^{-1/L}$, where L is vector lifespan [105].

(iii) Vector infectiousness

Virus infection, dissemination and infectiousness in the vector are temperature-dependent (figure 2*h*) [106]. We assumed that vector competence—the probability that a vector exposed to an infectious blood meal becomes infectious with virus in its salivary glands—is a quadratic function of temperature, as shown for other flaviviruses [107]. Additionally, we assumed that at a given temperature, the extrinsic incubation period—the length of time required for an exposed vector to become infectious—is log-normally distributed across individuals [108,109]. We fitted a Bayesian model using experimental data [110–117] with the package RStan [104].

(iv) Vector dispersal

To estimate the range over which sylvatic mosquitoes disperse (figure 2*f*), we fitted a negative binomial dispersal kernel [118] to mark–recapture data [119] using a Bayesian framework with the package RStan [104].

(v) Vector contacts

We approximated reservoir–vector contact (figure 2*c*) as per cent forest cover [120] contingent on the presence of at least one reservoir species (figure 2*a*). Similarly, we approximated human–vector contact (figure 2*d*) as per cent non-forest cover [120] contingent on the presence of human population (figure 2*j*).

(c) Phenomenological primate dynamics

Primate population dynamics and susceptibility have been suggested as important constraints on yellow fever spillover [19], which remain poorly characterized. In the absence of primate infection data, we assumed that human spillover events are a proxy for infection prevalence during reservoir

epizootics. This is the only mechanistic submodel that uses the human yellow fever spillover data directly—all other submodels are independent of human infection data. For this submodel, we used human cases of yellow fever reported by month of first symptoms and municipality of infection (2001–2016) from the Brazilian Ministry of Health [121]. We define a spillover municipality-month as one in which at least one human case of yellow fever occurred. As an estimate of reservoir infection dynamics, we fitted a phenomenological sine curve with a 7-year period [122] to the yearly number of municipality-months with spillover (figure 2*k*) and then transformed the curve to be positive and less than 1. The resulting curve is used as a spatially constant estimate of primate reservoir infection prevalence. Phenomenological primate dynamics are used in the periodic risk estimate (figure 2*o*) to account for a missing ecological process but are not used in any other risk metric, so all other risk metrics are parameterized independent of human spillover data.

(d) Model–data comparison

We compared spatially- and temporally-explicit mechanistic model predictions for spillover risk with observed human cases of yellow fever spillover using a statistical model. We limited the comparison to 2001–2016 based on the availability of human case data. We considered four modelled risk metrics (defined above): environmental risk, immunological risk, population-scaled risk and periodic risk. Because risk was modelled by pixel, to compare the model output with municipality-month observations of human cases, we calculate both mean risk and maximum risk in each municipality and month. While mean risk may be more representative of the entire municipality, we hypothesized that maximum risk in the municipality-month might better predict the small-scale processes that drive spillover. The use of maximum risk may also help to avoid spatial aggregation which can lead to bias or mask the relationships, for example the modifiable areal unit problem [123].

We compared municipality means and maxima for all four risk metrics with human yellow fever data for model evaluation in the following three ways. First, for each modelled risk metric and each municipality summary statistic (mean and maximum), we fitted a logistic regression of spillover probability as a function of model-predicted risk (electronic supplementary material, table S4) using glm in R [23]. Second, we calculated a receiver operating characteristic curve to calculate the area under the curve (AUC), a measure of goodness of fit, for each modelled risk metric and municipality summary statistic (electronic supplementary material, table S4). As this analysis focuses on prediction of spillover as a way to compare hypothesized mechanisms, comparison of AUC values with a null model is beyond the scope of this paper. Finally, for all eight mechanistic predictions and estimated vaccine coverage, we regressed the number of reported yellow fever cases given that spillover occurred, and calculated Spearman's rank correlation coefficient with number of reported cases to consider nonlinear but monotonic associations (electronic supplementary material, table S5).

(e) Statistical model

We used a boosted regression tree [124,125] to understand any potential gaps in the mechanistic model and its relationship to environmental and human population covariates. As predictors of yellow fever spillover in the boosted regression tree, we included the following covariates for each municipality-month: current and one-month lagged maximum predicted environmental risk, current and one-month lagged fire area, average and maximum number of primate species, estimated municipality vaccine coverage, average human population density, average monthly air temperature, average monthly precipitation, phenomenological primate dynamics, region and month (electronic supplementary material, table S6). Each observation is a municipality-month and the response variable is the binary indicator of whether or not yellow fever spillover occurred in a municipality-month (see Methods: Model–data comparison (§2d)). While some of predictor covariates contribute to the environmental risk metric (i.e., air temperature, rainfall and primate reservoir ranges), we also included them in the boosted regression tree analysis to identify whether the environmental covariates have any predictive power beyond their role in the mechanistic model, which could indicate that the mechanistic model does not fully capture their influence on spillover. We included fire area as a proxy for land conversion [126], which has previously been shown to be predictive of yellow fever spillover [8]. We also included vaccine coverage and human population density despite their poor predictive performance in the mechanistic model to identify whether these human population factors are predictive of spillover in ways not previously hypothesized, and therefore not captured in the mechanistic model. Boosted regression trees repeatedly fitted regression trees, which created multiple binary splits in the dataset based on predictor variables. Each successive tree was fitted to the residuals of the previous best model. The model was then updated to include the next tree [124]. Variable importance was calculated as a weighted sum of the number of times a variable was used for splitting, with weights determined by the squared improvement due to the split [124].

We fitted the boosted regression tree to data from 2001 to 2016, given this was the range of the available human case data for inferring spillover. We partitioned the dataset into spatially- and temporally-balanced training (80%) and test (20%) sets prior to the analysis. Optimal learning rate, tree complexity and number of trees were selected as the set of parameters that minimized cross-validation predictive deviance (electronic supplementary material, table S7; [124]). The dataset was split in R using the BalancedSampling package [127], models were fitted in R using the gbm and dismo [128,129] packages, and variable effects were calculated with the pdp package [130]. Additional details can be found in the electronic supplementary material.

3. Results

Primate species distribution (figure 2*a*), vector distribution (figure 2*b*; electronic supplementary material, figures S1 and S2), reservoir–vector contact (figure 2*c*), human–vector contact (figure 2*d*) and human susceptibility (figure 2*i*) varied over space and time based on estimates and models fitted to empirical data. In addition, vector survival (figure 2*g*) and infectiousness (figure 2*h*; electronic supplementary material, figures S4 and S5) varied with temperature, vector abundance varied seasonally with rainfall (figure 2*e*; electronic supplementary material, figure S3 and table S3), and vector dispersal declined exponentially with distance (figure 2*f*; electronic supplementary material, figure S6). Together, these empirical relationships between environment and host, vector and virus ecology compose an estimate of environmental risk of yellow fever spillover (electronic supplementary material, file S2).

The environmental risk model strongly predicted episodes of yellow fever spillover into humans (AUC = 0.72) and adding phenomenological reservoir infection dynamics in periodic risk further improved the model (AUC = 0.79; figure 3). Surprisingly, models that included human vaccination coverage and human population size performed worse than the environment-driven models (AUC = 0.64 and 0.64; figure 3). For all risk metrics, maximum value in the municipality-month was a better predictor of spillover than mean value (figure 3). Logistic regressions of

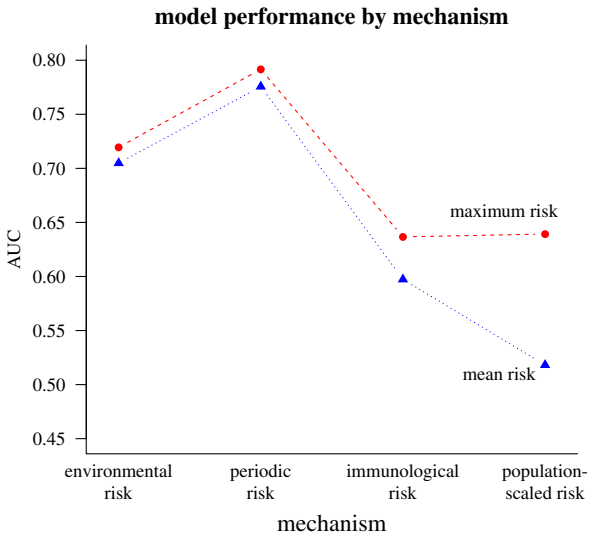

Figure 3. Municipality maximum periodic risk best predicts spillover. Each point is the calculated area under the curve (AUC) from spillover predicted by modelled risk, where higher AUC represents a model better able to distinguish between spillover and non-spillover observations. The risk models (from left to right on the *x*-axis) are environmental risk, periodic risk, immunological risk and population-scaled risk. Municipality-wide maxima (red dashed lines and circles) and means (blue dotted lines and triangles) are shown for each metric.

spillover probability as a function of model-predicted risk showed similar patterns in Akaike information criterion (AIC) values (electronic supplementary material, table S4). Model-predicted environmental (mean and maximum), periodic (mean and maximum) and immunological (maximum) risk metrics were statistically significant predictors of spillover probability at the 5% level after correcting for multiple hypothesis testing (electronic supplementary material, table S4; [131]). By contrast, given that spillover occurred, none of the eight mechanistic model risk summaries (maximum and mean of the four risk metrics) was a statistically significant predictor of number of cases, nor was estimated vaccine coverage (electronic supplementary material, table S5). In Spearman's rank correlations, we find that of the independent predictors, vaccine coverage is most correlated with risk, followed by maximum environmental risk, although these correlations are weak (electronic supplementary material, table S5).

Mechanistic model estimates matched seasonal variation in spillover, and accurately captured differences in seasonality by region (figure 4*a*). Risk peaked in April in the North and Northeast regions and in February in Central-West, South and Southeast regions. The seasonal regional correlation between number of municipality-months with spillover and average environmental risk was highest in the Southeast (0.77), followed by the South (0.61), Central- West (0.58) and North (0.42) regions. The periodic risk matched interannual variation in spillover (figure 4*c*), an unsurprising finding given periodic risk incorporated phenomenological primate dynamics derived from human cases of spillover. Interannual regional correlations were weaker than seasonal correlations but similarly highest in the Southeast (0.54), followed by the Central-West (0.45), North (0.21) and South (0.13) regions.

The boosted regression tree found one-month lagged environmental risk and current environmental risk to be the second and fifth most important predictors of spillover, respectively (figure 5). Not surprisingly, the boosted regression tree significantly improved predictive performance from the mechanistic model because it was trained on the human spillover data (training AUC > 0.99, test AUC $= 0.95$). Vaccine coverage, temperature, population density and precipitation were also among the six most important predictors in the boosted regression tree. As expected, municipality-months with spillover had higher current and one-month lagged environmental risk (figure 5*b*,*e*), as well as high (phenomenologically) estimated primate infection prevalence and high primate species richness (electronic supplementary material, figure S8). We find that municipality-months with spillover have low monthly average temperatures (figure 5*a*), which may in part be due to poorly captured effects of temperature in the mechanistic model from averaging temperature before calculating mosquito trait values for survival and infectiousness [132]. We also find that municipality-months with spillover have low rates of precipitation (figure 5*d*), which may correspond to settings with increased human activity in the forest, and therefore increased chance of spillover. However, current and lagged fire area, hypothesized indicators of deforestation activity, had low predictive importance in the boosted regression tree models (electronic supplementary material, figure S8).

Unexpectedly, municipality-months with spillover tended to have vaccine coverage above 90%, suggesting that high rates of vaccine coverage do not prevent spillover from occurring. While estimated vaccine coverage was included as a measure of human susceptibility, it is likely capturing other patterns in the spatial distribution of spillover; regions known to experience yellow fever spillover are likely to have high vaccination rates, while those where spillover is rare or non-existent are likely to have low vaccination rates. Accordingly, estimated vaccine coverage is bimodal, potentially due to a group of lower risk municipalities and a group of higher risk municipalities. The partial dependence plot also displays two plateaus in the marginal effect in the vaccine coverage on model estimates, which roughly correspond to the two vaccine coverage groups.

The recent outbreaks in Brazil in the 2016–2017 and 2017–2018 transmission seasons have been the largest in over 50 years [16]. The environmental risk model predicts persistent, low environmental risk of spillover in the affected states (Minas Gerais, Espírito Santo, São Paulo and Rio de Janeiro) and does not predict any increase in spillover risk during the recent transmission seasons (figure 6). The date ranges of confirmed human cases during the 2016–2017 and 2017–2018 outbreaks are shown in pink bands (figure 6) based on a World Health Organization epidemiological update [16]. The mechanistic model predicts spillover risk in Espírito Santo and Rio de Janeiro, where no spillover occurred from 2001 to 2016, at levels similar to those in Minas Gerais and São Paulo, where spillover had previously occurred. As in other regions, the model accurately captures the seasonality of spillover risk in this region (figure 6), which is distinct from that of other regions (figure 4*a*).

4. Discussion

Our mechanistic understanding of environmental risk of spillover—which combines reservoir host and sylvatic vector distributions, vector contact with reservoirs and

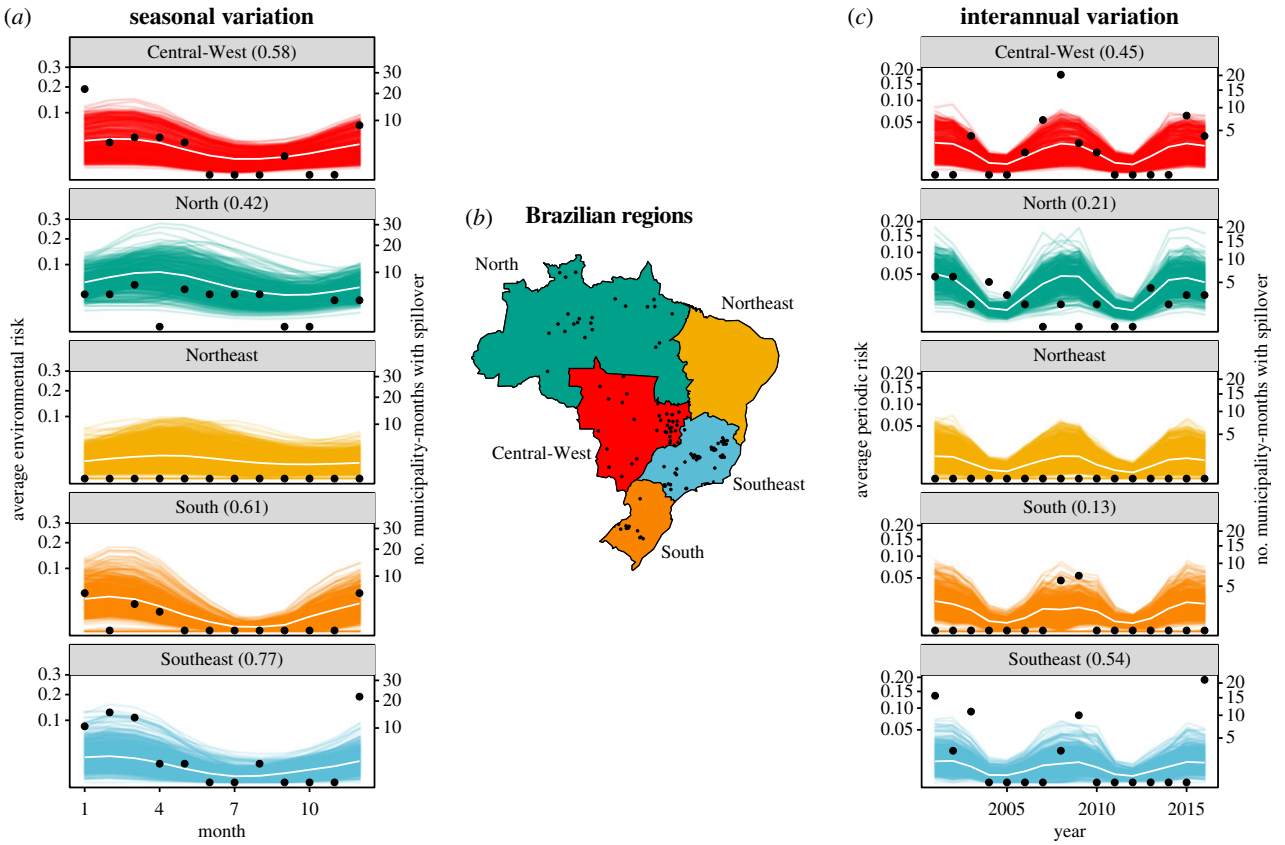

Figure 4. Modelled environmental risk captures seasonal variation and periodic risk captures interannual variation in spillover. Each coloured line is the seasonal average of modelled maximum environmental risk in a municipality (*a*) and the yearly average of modelled maximum periodic risk in a municipality (*c*). White lines are the regional average over the municipal curves. Black points represent the total number of municipality-months with spillover in that region per month (*a*) and per year (*c*), or the municipalities with at least one month with spillover (*b*). Correlations between regional average environmental risk (white lines) and regional number of municipality-months with spillover (black points) are shown in parentheses (*a*,*c*) for regions where spillover has occurred (all except the Northeast). Regions of Brazil are shown with corresponding colours (*b*). The Southeast (shown in blue) was the region with the majority of cases during the large outbreaks in 2016–2018. (Online version in colour.)

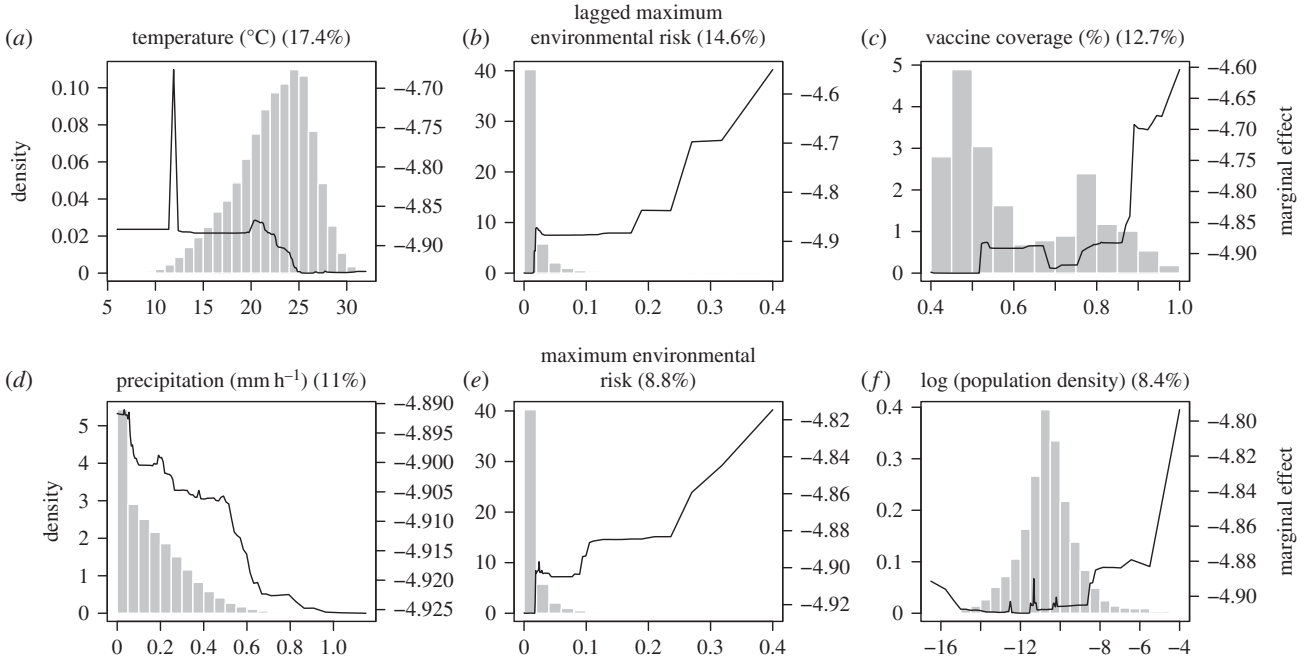

Figure 5. Partial dependence plots of top six predictors of spillover in a municipality-month from boosted regression tree analysis. Plots are listed in order of predictive importance with relative influence (%) listed. In order, the variables identified as most important predictors were average temperature in the municipality-month (*a*), one-month lagged maximum environmental risk (*b*), estimated vaccine coverage (*c*), average rate of precipitation in the municipality-month (*d*), current month maximum environmental risk (*e*) and municipality population density (log-scaled for visibility, *f*). Histograms show the distribution of observed municipality-months at each covariate value (left *y*-axis) and solid lines show the marginal effects of covariate on model prediction (right *y*-axis). Marginal effects highlight the characteristics of municipality-months that experienced spillover in Brazil 2001–2016.

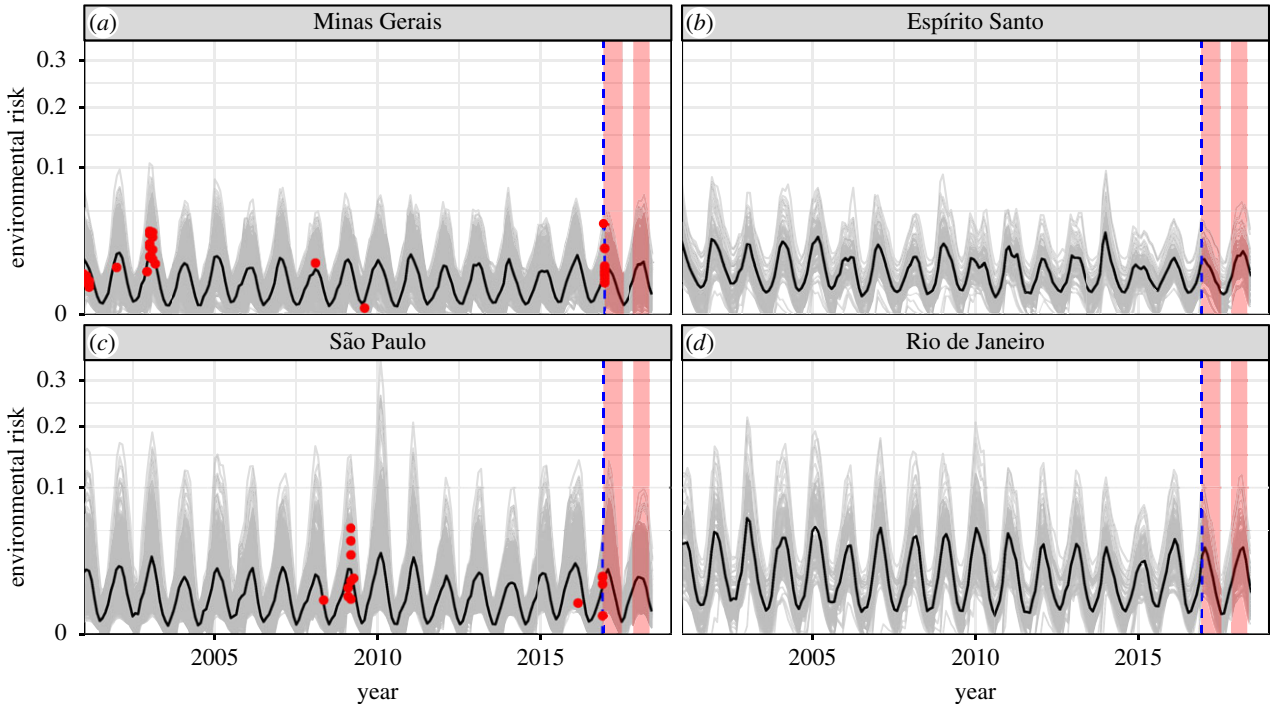

Figure 6. Mechanistic model predicts consistent low, seasonal risk across states in Southeast region of Brazil, where a large outbreak occurred in 2016–2018. Data are only available until the end of 2016 (blue dashed line), so do not include the duration of the 2016–2018 outbreaks (pink boxes). Only 2001–2016 spillovers are shown (red points), defined as municipality-months with human yellow fever cases. Red points show the date of spillover (*x*-axis) and modelled maximum environmental risk in the spillover municipality (*y*-axis). Grey lines are municipality estimates of maximum environmental risk and the black line is the environmental risk averaged over all municipalities in the state. Prior to the large outbreak in 2017–2018, spillover had occurred in Minas Gerais and São Paulo (*a*,*c*) but not in Espírito Santo or Rio de Janeiro (*b*,*d*). (Online version in colour.)

humans, and vector dispersal, survival, infectiousness and seasonal abundance—predicts yellow fever spillover into humans with high accuracy (AUC = 0.72; figure 3). Within each municipality and month, the maximum risk, rather than the mean risk, was the best predictor of spillover occurrence, suggesting that local heterogeneity in risk within municipalities is important for determining spillover probability. Rainfall-driven seasonality in the vector populations and temperature-driven seasonality in vector survival and infectiousness accurately predicted seasonal variation in spillover (figure 4*a*). While interannual variation in risk was not well-predicted in the environmental risk model based on climate and land cover information alone, including phenomenologically modelled variation in primate yellow fever infection prevalence improved predictions of year-to-year variation in spillover (AUC = 0.79).

Although we hypothesized that low vaccination coverage and high human population density would each increase spillover risk, neither improved model accuracy for predicting spillover in the mechanistic model (figure 3). However, we found that vaccine coverage was the third most important predictor of municipality-months with spillover when allowing for a nonlinear but generally positive relationship between coverage and spillover probability (figure 5).

The recent outbreak is also consistent with the ecological processes driving past spillover in this region (figure 6). While environmental risk in 2016–2018 was not elevated above historical levels (2001–2015) and spillover had not occurred in the states of Espírito Santo or Rio de Janeiro during the previous 15 years, it has previously occurred in Minas Gerais and São Paulo states in 2001–2003 and 2008–2009. Data from the recent 2016–2018 outbreak past December 2016 are not included in the statistical models because consistent monthly municipality-scale spillover data across the country are not available for that period.

The boosted regression tree analysis, which aimed to detect candidate drivers of spillover that might be missing from our mechanistic model, identified vaccine coverage, current and lagged environmental risk, temperature, population density and precipitation as important predictors, which together improved upon mechanistic model predictive performance of pathogen spillover (out-of-sample AUC = 0.95). The relative importance of lagged and current environmental risk provides evidence that the mechanistic model captures the potentially nonlinear and interactive relationship between environmental variables that drive spillover in mosquitoes, reservoir hosts and humans better than the environmental variables alone. One-month lagged environmental risk may be more important than current environmental risk for predicting spillover because of a lag between cases and reporting. Additionally, environmental suitability for reservoir and vectors may drive reservoir infection dynamics, causing a lag between conditions suitable for virus amplification in the primate reservoir and vector populations, and spillover into humans. Moreover, the relative importance of one-month lagged environmental risk creates the potential for forward prediction of spillover. The boosted regression tree also identified municipality-months with spillover to have low temperatures. As mosquito thermal performance traits often have steep drop-offs at high temperatures, temperature variation affects mosquito traits [133]. Our mechanistic model using monthly average temperature may overestimate the suitability in warm temperatures and underestimate the suitability in cool temperatures [132], resulting in the decreasing relationship observed between average monthly temperature and spillover in the boosted regression tree.

In a recent publication, Kaul *et al.* [8] also used a machine learning approach to predict municipality-months with spillover in Brazil and similarly found rainfall and temperature to be important predictors. However, their model also identified primate richness and fire density as important predictors, while our boosted regression tree analysis ranked municipality average primate richness tenth, municipality maximum primate richness fourteenth, one-month lagged fire area ninth, and current fire area twelfth for variable importance out of 14 variables. Our covariates add to those used by Kaul *et al.* [8] by including vaccine coverage and our mechanistic environmental risk estimate (current and lagged), which boosted regression trees found to be three of the five most important predictors. We expect that our mechanistic environmental risk estimates capture much of the variation attributed to other environmental variables in the Kaul *et al.* model. Despite the differing relative importance of variables for predicting spillover in the two models, they both predict that seasonal patterns vary by regions of Brazil and find Southeast Brazil seasonally suitable for yellow fever spillover. Our mechanistic model further illustrates that this differing seasonality can be explained by seasonal variation in vector survival and infectiousness driven by temperature and vector abundance driven by rainfall.

Given the importance of vaccination campaigns in limiting yellow fever outbreaks, we expected that the number of susceptible (unvaccinated) people would be an important positive predictor of yellow fever spillover occurrence, yet mechanistic population-scaled risk performed worse at predicting spillover than environmental risk alone (figure 3). For example, scaling by population size predicts areas of very high risk along the coast of Brazil, where environmental risk is low, but population sizes are high. Additionally, we expected that vaccination coverage and human density might be more predictive of the number of cases in spillover events (for example, the recent outbreak in Southeast Brazil) than the probability of spillover occurring, given that very low environmental suitability will be amplified in large, unvaccinated populations. However, vaccine coverage was not a significant predictor of the number of human cases of yellow fever given that spillover occurred (electronic supplementary material, table S5). Anecdotally, it is worth noting that prior to the recent large outbreak in southeastern Brazil in 2016–2018, vaccination rates in the region were low, potentially allowing that outbreak to reach an unusually high magnitude.

The substantial improvement in model prediction from environmental to periodic risk (AUC = 0.72 versus 0.79) suggests that primate population dynamics, immunity and infection prevalence may be a key missing component of this mechanistic model. Ongoing surveillance efforts in Brazil are used to detect non-human primate cases of yellow fever as an advanced warning system [134]. While this advanced warning system can make a critical difference, the recent outbreaks in Southeast Brazil displayed that in some cases this surveillance may not provide sufficient time to respond to prevent spillover, especially in areas with high populations and low vaccine coverage rates, as were found in the Southeast. Incorporating a mechanistic model of non-human primate infection prevalence, driven by local primate surveillance data, could help to indicate when primate cases of yellow fever are likely, to provide additional time for public health officials to respond. This remains a significant and potentially very fruitful gap in our understanding of yellow fever transmission and spillover.

Vector–human contact rates are another important empirical gap in the mechanistic model, which could further refine the relationships between land use, human occupations and behaviour, and spillover risk. We approximate human contact rates with sylvatic vectors with per cent forest cover, but the relationship is likely much more complex. The surprising decreasing relationship between precipitation and spillover probability in the boosted regression tree (figure 5*d*) may be due to the influence of precipitation on human activities in and around forests, and therefore its influence on human–vector contact [96]. Additionally, while vector contacts depend on biting rate of the vector, and mosquito biting rates are known to depend on temperature for other species [107,135], we assume constant biting rate in the mechanistic model owing to a lack of empirical evidence.

While beyond the scope of this paper, the most influential mechanisms in the model could be further identified through sensitivity analyses of specific submodel components. Additionally, associations between model components and spillover probability could be estimated using the framework of percolation models [17]. Finally, a thorough uncertainty analysis could highlight the model components most in need of further study to improve prediction of spillover.

Yellow fever is an ancient, historically important human disease that played a central role in the discovery of mosquito transmission of pathogens and the subsequent development of vector control as a public health measure [136]. The wealth of existing knowledge about the ecology of yellow fever virus and its sylvatic reservoir hosts and vectors allowed us to synthesize data from 71 published papers to mathematically formalize our ecological understanding of sylvatic transmission and spillover. Although spillover is a stochastic process that is expected to be difficult to predict, the mechanistic model which integrates vector, human host, non-human reservoir and virus ecology allowed us to predict spillover with surprising accuracy. Historically in the Americas and presently in other regions such as sub-Saharan Africa, yellow fever regularly has entered urban transmission cycles that lead to major human epidemics. The model framework presented here could be extended to include the ecology of different vectors, hosts and environments, including urban *Ae. aegypti* and more human immune interactions with other flaviviruses, to ask intriguing questions such as: What prevents yellow fever from entering urban transmission cycles in the Americas, where other flavivirus epidemics regularly occur? Why has urban transmission occurred recently in Africa and not in South America? What prevents yellow fever circulation and spillover in Southeast Asia, where sylvatic vectors and non-human primate hosts are present and the climate is suitable? Answers to these questions would further our understanding of the ecology of (re)emerging diseases in different parts of the world. More fundamentally, this work provides clear evidence for the predictive power of mechanistic, ecological models—even for rare events like pathogen spillover—and can provide useful information to enhance public health interventions of zoonotic diseases.

Data accessibility. All data and code are available on GitHub: https://github.com/marissachilds/YellowFeverSpillover.

Authors' contributions. M.L.C. and E.A.M. conceived of the project and designed the analyses. M.L.C., N.N. and J.C. collected the data and performed the analyses. N.N. created the artwork in figures 1 and 2. M.L.C. drafted the manuscript. E.A.M., N.N. and J.C. revised the manuscript and all authors read and approved the final manuscript.

Competing interests. We have no competing interests.

Funding. M.L.C. was funded by the Lindsay Family E-IPER Fellowship. N.N. was funded by the Bing Fellowship in Honor of Paul Ehrlich. J.C. was funded by the Stanford University Biology Summer Undergraduate Research Program. E.A.M. was funded by the National Science Foundation Ecology and Evolution of Infectious Diseases program (DEB-1518681), the Stanford University Woods Institute for the Environment—Environmental Ventures Program and the Hellman Faculty Fellowship.

Acknowledgements. Freya Shearer kindly provided data on vaccine coverage estimates. We thank the Defense Advanced Research Projects Agency, whose funding provided the opportunity to discuss and develop this project at a workshop on pathogen spillover. We also thank the authors of many previous studies who have made their data available, and we are grateful for the publicly available remote sensing data that made this project possible. The manuscript was improved by comments from anonymous reviewers.

References

1. Woolhouse MEJ, Haydon DT, Antia R. 2005 Emerging pathogens: the epidemiology and evolution of species jumps. *Trends Ecol. Evol.* **20**, 238–244. (doi:10.1016/j.tree.2005.02.009)
2. Jones KE, Patel NG, Levy MA, Storeygard A, Balk D, Gittleman JL, Daszak P. 2008 Global trends in emerging infectious diseases. *Nature* **451**, 990–993. (doi:10.1038/nature06536)
3. Plowright RK, Parrish CR, McCallum H, Hudson PJ, Ko AI, Graham AL, Lloyd-Smith JO. 2017 Pathways to zoonotic spillover. *Nat. Rev. Microbiol.* **15**, 502–510. (doi:10.1038/nrmicro.2017.45)
4. Plowright RK *et al.* 2014 Ecological dynamics of emerging bat virus spillover. *Proc. R. Soc. B* **282**, 20142124. (doi:10.1098/rspb.2014.2124)
5. Lloyd-Smith JO *et al.* 2009 Epidemic dynamics at the human-animal interface. *Science* **326**, 1362–1367. (doi:10.1126/science.1177345)
6. Hamrick PN, Aldighieri S, Machado G, Leonel DG, Vilca LM, Uriona S, Schneider MC. 2017 Geographic patterns and environmental factors associated with human yellow fever presence in the Americas. *PLoS Negl. Trop. Dis.* **11**, e5897. (doi:10.1371/journal.pntd.0005897)
7. Schmidt JP, Park AW, Kramer AM, Han BA, Alexander LW, Drake JM. 2017 Spatiotemporal fluctuations and triggers of Ebola virus spillover. *Emerg. Infect. Dis.* **23**, 415–422. (doi:10.3201/eid2303.160101)
8. Kaul RB, Evans MV, Murdock CC, Drake JM. 2018 Spatio-temporal spillover risk of yellow fever in Brazil. *Parasit. Vectors* **11**, 488. (doi:10.1186/s13071-018-3063-6)
9. Monath TP, Vasconcelos PFC. 2015 Yellow fever. *J. Clin. Virol.* **64**, 160–173. (doi:10.1016/j.jcv.2014.08.030)
10. Paules CI, Fauci AS. 2017 Yellow fever — once again on the radar screen in the Americas. *N. Engl. J. Med.* **376**, 1397–1399. (doi:10.1056/NEJMp1002530)
11. Faria NR *et al.* 2018 Genomic and epidemiological monitoring of yellow fever virus transmission potential. *Science* **361**, 894–899. (doi:10.1126/science.aat7115)
12. Hanley KA, Monath TP, Weaver SC, Rossi SL, Richman RL, Vasilakis N. 2013 Fever versus fever: the role of host and vector susceptibility and interspecific competition in shaping the current and future distributions of the sylvatic cycles of dengue virus and yellow fever virus. *Infect. Genet. Evol.* **19**, 292–311. (doi:10.1016/j.meegid.2013.03.008)
13. Johansson MA, Vasconcelos PFC, Staples JE. 2014 The whole iceberg: estimating the incidence of yellow fever virus infection from the number of severe cases. *Trans. R. Soc. Trop. Med. Hyg.* **108**, 482–487. (doi:10.1093/trstmh/tru092)
14. Valderrama A, Díaz Y, López-Vergès S. 2017 Interaction of Flavivirus with their mosquito vectors and their impact on the human health in the Americas. *Biochem. Biophys. Res. Commun.* **492**, 541–547. (doi:10.1016/j.bbrc.2017.05.050)
15. de Souza RP *et al.* 2010 Detection of a new yellow fever virus lineage within the South American genotype I in Brazil. *J. Med. Virol.* **82**, 175–185. (doi:10.1002/jmv.21606)
16. Pan American Health Organization/World Health Organization. 2018 *Epidemiological update: yellow fever (7 December 2018)*. See https://bit.ly/2Qhwucf.
17. Washburne AD, Crowley DE, Becker DJ, Manlove KR, Childs ML, Plowright RK. 2019 Percolation models of pathogen spillover. *Phil. Trans. R. Soc. B* **374**, 20180331. (doi:10.1098/rstb.2018.0331)
18. Shearer FM *et al.* 2017 Global yellow fever vaccination coverage from 1970 to 2016: an adjusted retrospective analysis. *Lancet Infect. Dis.* **17**, 1209–1217. (doi:10.1016/S1473-3099(17)30419-X)
19. Vasconcelos PFC. 2010 Yellow fever in Brazil: thoughts and hypotheses on the emergence in previously free areas. *Rev. Saude Publica* **44**, 1144–1149. (doi:10.1590/S0034-89102010005000046)
20. Gorelick N, Hancher M, Dixon M, Ilyushchenko S, Thau D, Moore R. 2017 Google Earth Engine: planetary-scale geospatial analysis for everyone. *Remote Sens. Environ.* **202**, 18–27. (doi:10.1016/j.rse.2017.06.031)
21. IUCN. 2018 *The IUCN red list of threatened species.* Version 2018-2. See http://www.iucnredlist.org (accessed 10 July 2018).
22. NASA Socioeconomic Data & Applications Center. 2016 *Gridded Population of the World, Version 4 (GPWv4): Population Count Adjusted to Match 2015 Revision of UN WPP Country Totals*. New York, NY: Center for International Earth Science Information Network (CIESIN), Columbia University. (doi:10.7927/H4SF2T42)
23. R Core Team. 2018 *R: a language and environment for statistical computing*. Vienna, Austria: R Foundation for Statistical Computing. See https://www.r-project.org/.
24. Wickham H. 2011 The split-apply-combine strategy for data analysis. *J. Stat. Softw.* **40**, 1–29. (doi:10.18637/jss.v040.i01)
25. Wickham H, François R, Henry L, Müller K. 2019 *dplyr: A Grammar of Data Manipulation*. See https://cran.r-project.org/package=dplyr.
26. Bache SM, Wickham H. 2014 *magrittr: A Forward-Pipe Operator for R*. See https://cran.r-project.org/package=magrittr.
27. Bivand R, Keitt T, Rowlingson B. 2018 *rgdal: Bindings for the 'Geospatial' Data Abstraction Library*. See https://cran.r-project.org/package=rgdal.
28. Wickham H. 2018 *stringr: Simple, Consistent Wrappers for Common String Operations*. See https://cran.r-project.org/package=stringr.
29. Hijmans RJ. 2018 *raster: Geographic Data Analysis and Modeling*. See https://cran.r-project.org/package=raster.
30. Wickham H. 2016 *Ggplot2: elegant graphics for data analysis*. New York: NY: Springer. See http://ggplot2.org.
31. Borchers HW. 2018 *pracma: Practical Numerical Math Functions*. See https://cran.r-project.org/package=pracma.
32. Bivand R, Rundel C. 2018 rgeos: Interface to Geometry Engine - Open Source ('GEOS'). See https://cran.r-project.org/package=rgeos.
33. Phillips SJ, Anderson RP, Schapire RE. 2006 Maximum entropy modeling of species geographic distributions. *Ecol. Modell.* **190**, 231–259. (doi:10.1016/j.ecolmodel.2005.03.026)
34. Elith J, Phillips SJ, Hastie T, Dudík M, Chee YE, Yates CJ. 2011 A statistical explanation of MaxEnt for ecologists. *Divers. Distrib.* **17**, 43–57. (doi:10.1111/j.1472-4642.2010.00725.x)
35. GBIF. 2018 GBIF occurrence download. (accessed 13 July 2018). (doi:10.15468/dl.gxbxtq)
36. GBIF. 2018 GBIF occurrence download. (accessed 13 July 2018). (doi:10.15468/dl.1uo4ty)
37. GBIF. 2018 GBIF occurrence download. (accessed 13 July 2018). (doi:10.15468/dl.ozsvnj)
38. Alencar J, de Mello CF, Gil-Santana HR, de Almeida SAS, Gleiser RM. 2016 Vertical oviposition activity of mosquitoes in the Atlantic Forest of Brazil with emphasis on the sylvan vector, *Haemagogus*

leucocelaenus (Diptera: Culicidae). *J. Vector Ecol.* **41**, 18–26. (doi:10.1111/jvec.12189)

39. Alencar J, De Mello VS, Serra-Freire NM, Silva JDS, Morone F, Guimarães AÉ. 2012 Evaluation of mosquito (Diptera: Culicidae) species richness using two sampling methods in the hydroelectric reservoir of Simplício, Minas Gerais, Brazil. *Zoologic Sci.* **29**, 218–222. (doi:10.2108/zsj.29.218)
40. Barbosa AA, Navarro-Silva MA, Calado D. 2003 Culicidae activity in a restrict forest inside Curitiba urban area (Paraná, Brazil). *Rev. Bras. Zool.* **20**, 59–63 (in Portuguese with English abstract). (doi:10.1590/S0101-81752003000100007)
41. Cardoso JC *et al.* 2010 Yellow fever virus in *Haemagogus leucocelaenus* and *Aedes serratus* mosquitoes, southern Brazil, 2008. *Emerg. Infect. Dis.* **16**, 1918–1924. (doi:10.3201/eid1612.100608)
42. Cardoso JDC *et al.* 2011 Ecological aspects of mosquitoes (Diptera: Culicidae) in an Atlantic forest area on the north coast of Rio Grande do Sul State, Brazil. *J. Vector Ecol.* **36**, 175–186. (doi:10.1111/j.1948-7134.2011.00155.x)
43. Chadee DD, Beier JC. 1996 Natural variation in blood-feeding kinetics of four mosquito vectors. *J. Vector Ecol.* **21**, 150–155.
44. Correa FF, Gleiser RM, Leite PJ, Fagundes E, Gil-Santana HR, Mello CF, Gredilha R, Alencar J. 2014 Mosquito communities in Nova Iguaçu Natural Park, Rio de Janeiro, Brazil. *J. Am. Mosq. Control Assoc.* **30**, 83–90. (doi:10.2987/13-6372.1)
45. D'Oria JM, Martí DA, Rossi GC. 2010 Culicidae, province of Misiones, northeastern Argentina. *Check List* **6**, 176–179. (doi:10.15560/6.1.176)
46. das Virgens TM, Rezende HR, Pinto IS, Falqueto A. 2018 Fauna of mosquitoes (Diptera: Culicidae) in Goytacazes National Forest and surrounding area, State of Espírito Santo, southeastern Brazil. *Biota Neotrop.* **18**, 250. (doi:10.1590/1676-0611-bn-2016-0250)
47. De Figueiredo ML *et al.* 2010 Mosquitoes infected with dengue viruses in Brazil. *Virol. J.* **7**, 152. (doi:10.1186/1743-422X-7-152)
48. de Souza RP *et al.* 2011 Isolation of yellow fever virus (YFV) from naturally infected *Haemagogus* (*Conopostegus*) *leucocelaenus* (Diptera, Culicidae) in São Paulo state, Brazil, 2009. *Rev. Inst. Med. Trop. Sao Paulo.* **53**, 133–139. (doi:10.1590/S0036-46652011000300004)
49. Dos Santos EB, Orlandin E, Piovesan M, Favretto MA. 2016 Short communication on the mosquitoes of a forested urban area at the municipality of Joaçaba, Santa Catarina, Brazil. *Entomotropica* **31**, 91–94.
50. Alencar J, Gil-Santana HR, Oliveira RDFND, Dgallier N, Guimares AR. 2010 Natural breeding sites for *Haemagogus* mosquitoes (Diptera, Culicidae) in Brazil. *Entomol News* **121**, 393–396. (doi:10.3157/021.121.0414)
51. Fernandez Z, Richartz R, Da Rosa AT, Soccol VT. 2000 Identification of the encephalitis equine virus, Brazil. *Rev. Saude Publica* **34**, 232–235. (doi:10.1590/S0034-89102000000300004)
52. Forattini OP, Gomes AD. 1988 Biting activity of *Aedes scapularis* (Rondani) and *Haemagogus* mosquitos in Southern Brazil (Diptera, Culicidae). *Rev. Saude Publica* **22**, 84–93. (doi:10.1590/S0034-89101988000200003)
53. Freitas SSO, de Mello CF, Figueiro R, Maia DA, Alencar J. 2018 Distribution of the mosquito communities (Diptera: Culicidae) in oviposition traps introduced into the Atlantic forest in the State of Rio de Janeiro, Brazil. *Vector-Borne Zoonotic Dis.* **18**, 214–221. (doi:10.1089/vbz.2017.2222)
54. Inácio CLS *et al.* 2017 Checklist of mosquito species (Diptera: Culicidae) in the Rio Grande do Norte state, Brazil—contribution of entomological surveillance. *J. Med. Entomol.* **54**, 763–773. (doi:10.1093/jme/tjw236)
55. Linares MA, Laurito M, Visintin AM, Rossi GC, Stein M, Almirón WR. 2016 New mosquito records (Diptera: Culicidae) from northwestern Argentina. *Check List* **12**, 1944. (doi:10.15560/12.4.1944)
56. Lira-Vieira AR *et al.* 2013 Ecological aspects of mosquitoes (Diptera: Culicidae) in the gallery forest of Brasilia National Park, Brazil, with an emphasis on potential vectors of yellow fever. *Rev. Soc. Bras. Med. Trop.* **46**, 566–574. (doi:10.1590/0037-8682-0136-2013)
57. Mangudo C, Aparicio JP, Rossi GC, Gleiser RM. 2018 Tree hole mosquito species composition and relative abundances differ between urban and adjacent forest habitats in northwestern Argentina. *Bull. Entomol. Res.* **108**, 203–212. (doi:10.1017/S0007485317000700)
58. Marassá AM, Paula MB, Gomes AC, Consales CA. 2009 Biotin-avidin sandwich ELISA with specific human isotypes IgG1 and IgG4 for Culicidae mosquito blood meal identification from an epizootic yellow fever area in Brazil. *J. Venom. Anim. Toxins Incl. Trop. Dis.* **15**, 696–706. (doi:10.1590/S1678-91992009000400008)
59. Medeiros-Sousa AR, Fernandes A, Ceretti-Junior W, Wilke ABB, Marrelli MT. 2017 Mosquitoes in urban green spaces: using an island biogeographic approach to identify drivers of species richness and composition. *Sci. Rep.* **7**, 17826. (doi:10.1038/s41598-017-18208-x)
60. Medeiros AS, Marcondes CB, De Azevedo PRM, Jerônimo SMR, Silva VPME, De Melo Ximenes MFFM. 2009 Seasonal variation of potential flavivirus vectors in an urban biological reserve in northeastern Brazil. *J. Med. Entomol.* **46**, 1450–1457. (doi:10.1603/033.046.0630)
61. Alencar J *et al.* 2014 A comparative study of the effect of multiple immersions on Aedini (Diptera: Culicidae) mosquito eggs with emphasis on sylvan vectors of yellow fever virus. *Mem. Inst. Oswaldo Cruz* **109**, 114–117. (doi:10.1590/0074-0276130168)
62. Méndez-López MR, Attoui H, Florin D, Calisher CH, Florian-Carrillo JC, Montero S. 2015 Association of vectors and environmental conditions during the emergence of Peruvian horse sickness orbivirus and Yunnan orbivirus in northern Peru. *J. Vector Ecol.* **40**, 355–363. (doi:10.1111/jvec.12174)
63. Montes J. 2005 Culicidae fauna of Serra da Cantareira, Sao Paulo, Brazil. *Rev. Saude Publica* **39**, 578–584. (doi:10.1590/S0034-89102005000400010)
64. Mucci LF *et al.* 2016 *Haemagogus leucocelaenus* and other mosquitoes potentially associated with sylvatic yellow fever in Cantareira State Park in the São Paulo Metropolitan Area, Brazil. *J. Am. Mosq. Control Assoc.* **32**, 329–332. (doi:10.2987/16-6587.1)
65. Muller GA, Dalavequia MA, Wagner G, Marcondes CB. 2014 Blood sucking Diptera (Culicidae, Psychodidae, Simuliidae) in forest fragment under impact of dam in the borderland of Rio Grande do Sul and Santa Catarina states, Brazil. *Cienc. Rural.* **44**, 1194–1196. (doi:10.1590/0103-8478cr20131656)
66. Müller GA, Kuwabara EF, Duque JE, Navarro-Silva MA, Marcondes CB. 2008 New records of mosquito species (Diptera: Culicidae) for Santa Catarina and Paraná (Brazil). *Biota Neotrop.* **8**, 211–218. (doi:10.1590/S1676-06032008000400021)
67. Orlandin E, Santos EB, Piovesan M, Favretto MA, Schneeberger AH, Souza VO, Muller GA, Wagner G. 2017 Mosquitoes (Diptera: Culicidae) from crepuscular period in an Atlantic Forest area in Southern Brazil. *Braz. J. Biol.* **77**, 60–67. (doi:10.1590/1519-6984.09815)
68. Pauvolid-Corrêa A *et al.* 2010 Preliminary investigation of Culicidae species in South Pantanal, Brazil and their potential importance in arbovirus transmission. *Rev. Inst. Med. Trop. Sao Paulo* **52**, 17–23. (doi:10.1590/S0036-46652010000100004)
69. Pecor JE *et al.* 2000 Annotated checklist of the mosquito species encountered during arboviral studies in Iquitos, Peru (Diptera: Culicidae). *J. Am. Mosq. Control Assoc.* **16**, 210–218.
70. Pinto CS, Confalonieri UEC, Mascarenhas BM. 2009 Ecology of *Haemagogus* sp. and *Sabethes* sp. (Diptera: Culicidae) in relation to the microclimates of the Caxiuanã National Forest, Pará, Brazil. *Mem. Inst. Oswaldo Cruz* **104**, 592–598. (doi:10.1590/S0074-02762009000400010)
71. Rossi GC. 2015 Annotated checklist, distribution, and taxonomic bibliography of the mosquitoes (Insecta: Diptera: Culicidae) of Argentina. *Check List* **11**. (doi:10.15560/11.4.1712)
72. Alencar J, Morone F, Mello CFD, Dégallier N, Lucio PS, Serra-Freire NMD. 2013 Flight height preference for oviposition of mosquito (Diptera: Culicidae) vectors of sylvatic yellow fever virus near the hydroelectric reservoir of Simplicío, Minas Gerais, Brazil. *J. Med. Entomol.* **50**, 791–795. (doi:10.1603/ME12120)
73. Rubio-Palis Y *et al.* 2010 Ecological characterization of anophelines and culicines in the indigenous territory of the Lower Caura River, Bolívar State, Venezuela. *Bol. Malariol. Salud Ambient.* **50**, 95–107.
74. Santos CF, Borges M. 2015 Impact of livestock on a mosquito community (Diptera: Culicidae) in a Brazilian tropical dry forest. *Rev. Soc. Bras. Med. Trop.* **48**, 474–478. (doi:10.1590/0037-8682-0022-2015)
75. Santos CF, Silva AC, Rodrigues RA, Jesus JSR, Borges MAZ. 2015 Inventory of mosquitoes (Diptera: Culicidae) in conservation units in Brazilian tropical dry forests. *Rev. Inst. Med. Trop. Sao Paulo* **57**, 227–232. (doi:10.1590/S0036-46652015000300008)

76. Serra OP, Cardoso BF, Ribeiro ALM, Leal dos Santos FA, SIhessarenko RD. 2016 Mayaro virus and dengue virus 1 and 4 natural infection in culicids from Cuiaba, state of Mato Grosso, Brazil. *Mem. Inst. Oswaldo Cruz* **111**, 20–29. (doi:10.1590/0074-02760150270)
77. Silva JDS, Pacheco JB, Alencar J, Guimarães AÉ. 2010 Biodiversity and influence of climatic factors on mosquitoes (Diptera: Culicidae) around the Peixe Angical hydroelectric scheme in the state of Tocantins, Brazil. *Mem. Inst. Oswaldo Cruz* **105**, 155–162. (doi:10.1590/S0074-02762010000200008)
78. Talaga S, Dejean A, Carinci R, Gaborit P, Dusfour I, Girod R. 2015 Updated checklist of the mosquitoes (Diptera: Culicidae) of French Guiana. *J. Med. Entomol.* **52**, 770–782. (doi:10.1093/jme/tjv109)
79. Talaga S, Murienne J, Dejean A, Leroy C. 2015 Online database for mosquito (Diptera, Culicidae) occurrence records in French Guiana. *Zookeys* **2015**, 107–115. (doi:10.3897/zookeys.532.6176)
80. Tatila-Ferreira A, Maia DA, Alencar J. 2017 Development of preimaginal stages of *Haemagogus leucocelaenus* (Diptera: Culicidae) in laboratory conditions. *Entomol. News* **127**, 142–150. (doi:10.3157/021.127.0209)
81. Tatila-Ferreira A, Maia DA, Santos de Abreu FV, Rodrigues WC, Alencar J. 2017 Oviposition behavior of *Haemagogus leucocelaenus* (Diptera: Culicidae), a vector of wild yellow fever in Brazil. *Rev. Inst. Med. Trop. Sao Paulo* **59**, e60. (doi:10.1590/S1678-9946201759060)
82. Tubaki RM, Menezes RMT, Vesgueiro FT, Cardoso RP. 2010 Observations on *Haemagogus janthinomys* Dyar (Diptera: Culicidae) and other mosquito populations within tree holes in a gallery forest in the northwestern region of Sao Paulo state, Brazil. *Neotrop. Entomol.* **39**, 664–670. (doi:10.1590/S1519-566X2010000400030)
83. Alencar J, Serra-Friere NM, Marcondes CB, Silva JDS, Correa FF, Guimarães AE. 2010 Influence of climatic factors on the population dynamics of *Haemagogus janthinomys* (Diptera: Culicidae), a vector of sylvatic yellow fever. *Entomol. News* **121**, 45–52. (doi:10.3157/021.121.0109)
84. Alencar J, de Mello CF, Barbosa LS, Gil-Santana HR, Maia DA, Marcondes CB, Silva JS. 2016 Diversity of yellow fever mosquito vectors in the Atlantic forest of Rio de Janeiro, Brazil. *Rev. Soc. Bras. Med. Trop.* **49**, 351–356. (doi:10.1590/0037-8682-0438-2015)
85. Alencar J, Marcondes CB, Serra-Freire NM, Lorosa ES, Pacheco JB, Guimarães AÉ. 2008 Feeding patterns of *Haemagogus capricornii* and *Haemagogus leucocelaenus* (Diptera: Culicidae) in two Brazilian States (Rio de Janeiro and Goiás). *J. Med. Entomol.* **45**, 873–876. (doi:10.1093/jmedent/45.5.873)
86. Aragão A, Nunes NJP, Cruz ACR, Casseb SMM, Cardoso JF, da Silva SP, Ishikawa EAY. In press. Description and phylogeny of the mitochondrial genome of *Sabethes chloropterus*, *Sabethes glaucodaemon* and *Sabethes belisarioi* (Diptera: Culicidae). *Genomics.* (doi:10.1016/j.ygeno.2018.03.016)
87. Aragão NC, Müller GA, Balbino VQ, Lima Costa Jr CR, Figueirêdo Jr CS, Alencar J, Marcondes CB. 2010 A list of mosquito species of the Brazilian State of Pernambuco, including the first report of *Haemagogus janthinomys* (Diptera: Culicidae), yellow fever vector and 14 other species (Diptera: Culicidae). *Rev. Soc. Bras. Med. Trop.* **43**, 458–459. (doi:10.1590/S0037-86822010000400024)
88. Vale Barbosa MG *et al.* 2008 Record of epidemiologically important Culicidae in the rural area of Manaus, Amazonas. *Rev. Soc. Bras. Med. Trop.* **41**, 658–663. (doi:10.1590/S0037-86822008000600019)
89. Vasconcelos PFC *et al.* 2001 Yellow fever in Pará State, Amazon region of Brazil, 1998–1999: entomologic and epidemiologic findings. *Emerg. Infect. Dis.* **7**, 565–569. (doi:10.3201/eid0707.017738)
90. Vasconcelos PFC *et al.* 2003 Isolations of yellow fever virus from *Haemagogus leucocelaenus* in Rio Grande do Sul State, Brazil. *Trans. R. Soc. Trop. Med. Hyg.* **97**, 60–62. (doi:10.1016/S0035-9203(03)90023-X)
91. Yanoviak SP, Lounibos LP, Weaver SC. 2006 Land use affects macroinvertebrate community composition in phytotelmata in the Peruvian Amazon. *Ann. Entomol. Soc. Am.* **99**, 1172–1181. (doi:10.1603/0013-8746(2006)99[1172:LUAMCC]2.0.CO;2)
92. Zequi JAC, Lopes J, Medri IM. 2005 Immature specimens of Culicidae (Diptera) found in installed recipients in forest fragments in the Londrina, Paraná, Brazil. *Rev. Bras. Zool.* **22**, 656–661. (doi:10.1590/S0101-81752005000300021)
93. Phillips S. 2017 *maxnet: Fitting 'Maxent' Species Distribution Models with 'glmnet'*. See https://cran.r-project.org/package=maxnet.
94. GBIF. 2018 GBIF occurrence download. (accessed 19 July 2018). (doi:10.15468/dl.wvs9g2)
95. Fox SJ, Bellan SE, Perkins TA, Johansson MA, Meyers LA. 2019 Downgrading disease transmission risk estimates using terminal importations. *PLoS Negl. Trop. Dis.* **13**, e0007395. (doi:10.1371/journal.pntd.0007395)
96. Kumm HW. 1950 Seasonal variations in rainfall: prevalence of *Haemagogus* and incidence of jungle yellow fever in Brazil and Colombia. *Trans. R. Soc. Trop. Med. Hyg.* **43**, 673–682. (doi:10.1016/0035-9203(50)90009-5)
97. Causey OR, Dos Santos GV. 1949 Diurnal mosquitoes in an area of small residual forests in Brazil. *Ann. Entomol. Soc. Am.* **42**, 471–482. (doi:10.1093/aesa/42.4.471)
98. Chadee DD. 1990 Seasonal abundance and diel landing periodicity of *Sabethes chloropterus* (Diptera: Culicidae) in Trinidad, West Indies. *J. Med. Entomol.* **27**, 1041–1044. (doi:10.1093/jmedent/27.6.1041)
99. Chadee DD, Tikasingh ES, Ganesh R. 1992 Seasonality, biting cycle and parity of the yellow fever vector mosquito *Haemagogus janthinomys* in Trinidad. *Med. Vet. Entomol.* **6**, 143–148. (doi:10.1111/j.1365-2915.1992.tb00592.x)
100. Chadee DD, Ganesh R, Hingwan JO, Tikasingh ES. 1995 Seasonal abundance, biting cycle and parity of the mosquito *Haemagogus leucocelaenus* in Trinidad, West Indies. *Med. Vet. Entomol.* **9**, 372–376. (doi:10.1111/j.1365-2915.1995.tb00006.x)
101. Bates M. 1947 The development and longevity of *Haemagogus* mosquitoes under laboratory conditions. *Ann. Entomol. Soc. Am.* **40**, 1–12. (doi:10.1093/aesa/40.1.1)
102. Galindo P. 1958 Bionomics of *Sabethes chloropterus* Humboldt, a Vector of Sylvan Yellow Fever in Middle America. *Am. J. Trop. Med. Hyg.* **7**, 429–440. (doi:10.4269/ajtmh.1958.7.429)
103. Dégallier N *et al.* 1998 Release–recapture experiments with canopy mosquitoes in the genera *Haemagogus* and *Sabeihes* (Diptera: Culicidae) in Brazilian Amazonia. *J. Med. Entomol.* **35**, 931–936. (doi:10.1093/jmedent/35.6.931)
104. Team SD. 2018 RStan: the R interface to Stan. See http://mc-stan.org/.
105. Clements AN, Paterson GD. 1981 The analysis of mortality and survival rates in wild populations of mosquitoes. *J. Appl. Ecol.* **18**, 373. (doi:10.2307/2402401)
106. Tesla B, Demakovsky LR, Mordecai EA, Ryan SJ, Bonds MH, Ngonghala CN, Brindley MA, Murdock CC. 2018 Temperature drives Zika virus transmission: evidence from empirical and mathematical models. *Proc. R. Soc. B* **285**, 20180795. (doi:10.1098/rspb.2018.0795)
107. Mordecai EA *et al.* 2017 Detecting the impact of temperature on transmission of Zika, dengue, and chikungunya using mechanistic models. *PLoS Negl. Trop. Dis.* **11**, e0005568. (doi:10.1371/journal.pntd.0005568)
108. Johansson MA, Arana-Vizcarrondo N, Biggerstaff BJ, Staples JE. 2010 Incubation periods of yellow fever virus. *Am. J. Trop. Med. Hyg.* **83**, 183–188. (doi:10.4269/ajtmh.2010.09-0782)
109. Chan M, Johansson MA. 2012 The incubation periods of dengue viruses. *PLoS ONE* **7**, e50972. (doi:10.1371/journal.pone.0050972)
110. Kumm HW, Waddell MB. 1948 *Haemagogus capricornii* Lutz as a laboratory vector of yellow fever. *Am. J. Trop. Med. Hyg.* **s1-28**, 247–252. (doi:10.4269/ajtmh.1948.s1-28.247)
111. Roca-García M, Bates M. 1946 The development of the virus of yellow fever in *Haemagogus* mosquitoes. *Am. J. Trop. Med. Hyg.* **s1-26**, 585–605. (doi:10.4269/ajtmh.1946.s1-26.585)
112. Anderson CR, Osorno-Mesa E. 1946 The laboratory transmission of yellow fever virus by *Haemagogus splendens*. *Am. J. Trop. Med. Hyg.* **26**, 613–618. (doi:10.4269/ajtmh.1946.s1-26.613)
113. Waddell MB, Taylor RM. 1945 Studies on cyclic passage of yellow fever virus in South American mammals and mosquitoes: marmosets (*Callithrix aurita*) and cebus monkeys (*Cebus versutus*) in combination with *Aedes aegypti* and *Haemagogus equinus*. *Am. J. Trop. Med. Hyg.* **s1-25**, 225–230. (doi:10.4269/ajtmh.1945.s1-25.225)
114. Roca-Garcia M, Bates M. 1945 Laboratory studies of the saimiri-*Haemagogus* cycle of jungle yellow fever. *Am. J. Trop. Med. Hyg.* **s1-25**, 203–216. (doi:10.4269/ajtmh.1945.s1-25.203)
115. Galindo P, Trapido H, de Rodaniche E. 1956 Experimental transmission of yellow fever by Central American species of *Haemagogus* and *Sabethes*

chloropterus. *Am. J. Trop. Med. Hyg.* **5**, 1022–1031. (doi:10.4269/ajtmh.1956.5.1022)
116. Waddell MB. 1949 Comparative efficacy of certain South American *Aëdes* and *Haemagogus* mosquitoes as laboratory vectors of yellow fever. *Am. J. Trop. Med. Hyg.* **29**, 567–575. (doi:10.4269/ajtmh.1949.s1-29.567)
117. Waddell MB, Taylor RM. 1947 Studies on the cyclic passage of yellow fever virus in South American mammals and Mosquitoes III. Further observations on *Haemagogus equinus* as a vector of the virus. *Am. J. Trop. Med. Hyg.* **s1-27**, 471–476. (doi:10.4269/ajtmh.1947.s1-27.471)
118. Estep LK, Burkett-Cadena ND, Hill GE, Unnasch RS, Unnasch TR. 2010 Estimation of dispersal distances of *Culex erraticus* in a focus of eastern equine encephalitis virus in the southeastern United States. *J. Med. Entomol.* **47**, 977–986. (doi:10.1603/ME10056)
119. Causey OR, Kumm HW. 1948 Dispersion of forest mosquitoes in Brazil; preliminary studies. *Am. J. Trop. Med. Hyg.* **28**, 469–480. (doi:10.4269/ajtmh.1948.s1-28.469)
120. Dimiceli C, Carroll M, Sohlberg R, Kim DH, Kelly M, Townshend JRG. 2015 *MOD44B MODIS/Terra vegetation continuous fields yearly L3 global 250 m SIN grid V006*. Sioux Falls, SD: NASA EOSDIS Land Processes DAAC. (doi:10.5067/MODIS/MOD44B.006)
121. Ministério da Saúde do Brasil. 2017 *Epidemiológicas e morbidade* (in Portuguese). See http://www2.datasus.gov.br/DATASUS/index.php?area=0203 (accessed 18 October 2018).
122. Camara FP, Gomes ALBB, Carvalho LMF, Castello LGV. 2011 Dynamic behavior of sylvatic yellow fever in Brazil (1954-2008). *Rev. Soc. Bras. Med. Trop.* **44**, 297–299. (doi:10.1590/S0037-86822011005000024)
123. Dark SJ, Bram D. 2007 The modifiable areal unit problem (MAUP) in physical geography. *Prog. Phys. Geog. Earth Environ.* **31**, 471–479. (doi:10.1177/0309133307083294)
124. Elith J, Leathwick JR, Hastie T. 2008 A working guide to boosted regression trees. *J. Anim. Ecol.* **77**, 802–813. (doi:10.1111/j.1365-2656.2008.01390.x)
125. Han BA, Schmidt JP, Alexander LW, Bowden SE, Hayman DTS, Drake JM. 2016 Undiscovered bat hosts of filoviruses. *PLoS Negl. Trop. Dis.* **10**, e0004815. (doi:10.1371/journal.pntd.0004815)
126. Millones M, Rogan J, Turner II BL, Parmentier B, Harris R, Griffith D. 2017 Fire data as proxy for anthropogenic landscape change in the Yucatán. *Land* **6**, 61. (doi:10.3390/land6030061)
127. Grafström A, Lisic J. 2018 *BalancedSampling: Balanced and Spatially Balanced Sampling*. See https://cran.r-project.org/package=BalancedSampling
128. Greenwell B, Boehmke B, Cunningham J, GBM Developers. 2018 *gbm: Generalized Boosted Regression Models*. See https://cran.r-project.org/package=gbm.
129. Hijmans RJ, Phillips S, Leathwick J, Elith J. 2017 *dismo: Species Distribution Modeling*. See https://cran.r-project.org/package=dismo.
130. Greenwell BM. 2017 pdp: An R package for constructing partial dependence plots. *R J.* **9**, 421–436. (doi:10.32614/RJ-2017-016)
131. Goeman JJ, Solari A. 2014 Multiple hypothesis testing in genomics. *Stat. Med.* **33**, 1946–1978. (doi:10.1002/sim.6082)
132. Bernhardt JR, Sunday JM, Thompson PL, O'Connor MI. 2018 Nonlinear averaging of thermal experience predicts population growth rates in a thermally variable environment. *Proc. R. Soc. B* **285**, 20181076. (doi:10.1098/rspb.2018.1076)
133. Paaijmans KP, Blanford S, Bell AS, Blanford JI, Read AF, Thomas MB. 2010 Influence of climate on malaria transmission depends on daily temperature variation. *Proc. Natl Acad. Sci. USA* **107**, 15 135–15 139. (doi:10.1073/pnas.1006422107)
134. Almeida MAB *et al.* 2014 Surveillance for yellow fever virus in non-human primates in southern Brazil, 2001–2011: a tool for prioritizing human populations for vaccination. *PLoS Negl. Trop. Dis.* **8**, e0002741. (doi:10.1371/journal.pntd.0002741)
135. Shapiro LLM, Whitehead SA, Thomas MB. 2017 Quantifying the effects of temperature on mosquito and parasite traits that determine the transmission potential of human malaria. *PLoS Biol.* **15**, e2003489. (doi:10.1371/journal.pbio.2003489)
136. Gorgas WC. 1915 *Sanitation in Panama*. New York, NY: Appleton.